

# RSC Advances



This is an *Accepted Manuscript*, which has been through the Royal Society of Chemistry peer review process and has been accepted for publication.

*Accepted Manuscripts* are published online shortly after acceptance, before technical editing, formatting and proof reading. Using this free service, authors can make their results available to the community, in citable form, before we publish the edited article. This *Accepted Manuscript* will be replaced by the edited, formatted and paginated article as soon as this is available.

You can find more information about *Accepted Manuscripts* in the [Information for Authors](#).

Please note that technical editing may introduce minor changes to the text and/or graphics, which may alter content. The journal's standard [Terms & Conditions](#) and the [Ethical guidelines](#) still apply. In no event shall the Royal Society of Chemistry be held responsible for any errors or omissions in this *Accepted Manuscript* or any consequences arising from the use of any information it contains.

1 **Magnetic Fe<sub>3</sub>O<sub>4</sub>@MOFs decorated graphene nanocomposites as**  
2 **novel electrochemical sensor for ultrasensitive detection of**  
3 **dopamine**

4 Yang Wang, Yun Zhang \*, Chen Hou, Mingzhu Liu\*

5 *State Key Laboratory of Applied Organic Chemistry, Key Laboratory of Nonferrous Metal*

6 *Chemistry and Resources Utilization of Gansu Province, College of Chemistry and Chemical*

7 *Engineering, College of Resources and Environment, Institute of Biochemical Engineering*

8 *&Environmental Technology, Lanzhou University, Lanzhou 730000, China*

9 **Abstract**

10 A novel hybrid nanocomposite of magnetic Fe<sub>3</sub>O<sub>4</sub>@ZIF-8 (zeolitic imidazolate  
11 framework-8 coated Fe<sub>3</sub>O<sub>4</sub> nanocomposites denoted as Fe<sub>3</sub>O<sub>4</sub>@ZIF-8) decorated  
12 RGO (reduced graphite oxide) was prepared by a simple method for the first time and  
13 denoted as Fe<sub>3</sub>O<sub>4</sub>@ZIF-8/RGO. After the Fe<sub>3</sub>O<sub>4</sub>/RGO was formed by solvothermal  
14 approach, the MOFs (ZIF-8) was coated on the surface of Fe<sub>3</sub>O<sub>4</sub> to get the  
15 Fe<sub>3</sub>O<sub>4</sub>@ZIF-8/RGO nanocomposite. The resulted Fe<sub>3</sub>O<sub>4</sub>@ZIF-8/RGO nanocomposite  
16 was characterized by means of the transmission electron microscope (TEM), scanning  
17 electron microscopy (SEM), Fourier transform infrared spectra (FT-IR), X-ray  
18 diffraction spectrometry (XRD), X-ray photoelectron (XPS), and vibrating sample  
19 magnetometer (VSM). This nanocomposite was modified on the glassy carbon  
20 electrode to fabricate biosensor which used to electrochemical determination for  
21 dopamine (DA) in phosphate buffer solution. The results demonstrated the fabricated

---

\*Corresponding author. Fax: 86-931-8912113; *E-mail address:* zhangyun@lzu.edu.cn (Y. Zhang)

\*Corresponding author. Fax: 86-931-8912582; *E-mail address:* mzliu@lzu.edu.cn (M.Z. Liu)

22 biosensor showed great potential applications in the detection of DA with remarkable  
23 enhanced effect on voltammetric response of DA. The linear relationship between the  
24 response peak currents and DA concentration was in range from  $2.0 \times 10^{-9}$  to  $1.0 \times 10^{-5}$   
25 M, the limits of detection is  $6.67 \times 10^{-10}$  M.. Moreover, the prepared biosensor also  
26 showed good selectivity for DA detection in the presence of ascorbic acid and uric  
27 acid and satisfactory result in real samples detection.

## 28 **1.Introduction**

29 Metal-organic frameworks (MOFs), as a new kinds of structured hybrid materials  
30 that consist of inorganic connectors and organic linker molecules, have attracted  
31 enormous interest because of their large accessible surface areas, high porosity,  
32 tunable pore sizes, ordered crystalline structures and excellent mechanical stability.<sup>1-3</sup>  
33 These remarkable characteristics helped MOFs showed great potential application in  
34 gas adsorption, catalysis, separation and purification.<sup>4</sup> Because many metal ions used  
35 in MOFs are electrochemically active, MOFs are also received growing concerns in  
36 electrochemical biosensors field.<sup>5,6</sup> To enhance the conductivity, stability in aqueous  
37 solution and electro-catalytic activities of target analytes, the introduction of the other  
38 highly conductive and mechanically durable materials into MOFs has been  
39 proposed.<sup>7,8</sup>

40 Graphene, composed of a single-atom-thick two-dimensional sheet of covalently  
41 bonded carbon atoms, has extraordinary electronic conductivity, high specific surface  
42 area, exceptional electron transfer rate, optical, structural and mechanical  
43 properties.<sup>9-11</sup> In recent years, the graphene has been pay close attention to be the

44 outstanding candidate for potential electrode modifying material because its  
45 bio-electrocatalytic properties and physical stability.<sup>12, 13</sup> As one kind of chemically  
46 derived graphene, reduced graphite oxide (RGO) with similar characteristics to  
47 graphene in many aspects has shown great utilization potentiality for application as  
48 highly sensitive biosensors.<sup>14</sup> To overcome the poor dispersibility and being prone to  
49 aggregation owing to the strong stacking tendency in the synthesis process of  
50 bulk-quantity RGO, decorating the RGO nano-sheets with inorganic nanoparticles  
51 during the preparation is the reasonable way which not only decreases restacking for  
52 RGO nano-sheets but also enhances the physical and chemical properties.<sup>15</sup>

53 Dopamine (DA) is one of the most significant and representative catecholamine  
54 neurotransmitter mediating the transmission of messages within the central nervous  
55 system of mammals and humans. An abnormal dopaminergic neuron process may  
56 lead to neurological illnesses, such as Parkinson's, Alzheimer's and Schizophrenia  
57 diseases.<sup>16</sup> As the trace level concentration of DA change has been related to various  
58 diseases, the rapid, sensitive and accurate measurement to detect the trace amount of  
59 DA is of extreme importance. Several methods have been established for DA  
60 detection, such as liquid chromatography, chemiluminescence, capillary  
61 electrophoresis, fluorescence, and absorbance and colorimetric methods. Because DA  
62 can be easily electrochemically oxidized, the electrochemical biosensors have been  
63 considered to be superior to other techniques for the determination of DA in view of  
64 its high accuracy, fast response, bulk modification with simple instruments, and low  
65 operation and instrumental expenses.<sup>17</sup>

66 Zeolitic imidazolate frameworks (ZIFs) is an attractive subfamily of MOFs due to  
67 their exceptional chemical and thermal stabilities and the ease of synthesis. In this  
68 work, we have developed a simple method to prepare a novel hybrid nanocomposite  
69 of magnetic Fe<sub>3</sub>O<sub>4</sub>@ZIF-8 decorated graphene with excellent dispersibility and  
70 stability in aqueous solution.<sup>18</sup> In this process, Fe<sub>3</sub>O<sub>4</sub> decorated RGO is formed firstly  
71 by the solvothermal approach, and then ZIF-8 is synthesized on the surface of Fe<sub>3</sub>O<sub>4</sub>  
72 to get the final products, Fe<sub>3</sub>O<sub>4</sub>@ZIF-8/RGO nanocomposite. The designed novel  
73 structure of anchoring the Fe<sub>3</sub>O<sub>4</sub>@MOFs nanospheres on graphene nano-sheets could  
74 not only restrained restacking of the graphene nano-sheets, but also incorporated of a  
75 rapid response towards an assistant magnetic field and fascinating electro-catalytic  
76 properties. To explore the potential electrochemical application of the  
77 Fe<sub>3</sub>O<sub>4</sub>@ZIF-8/RGO, the nanocomposite was immobilized on a glassy carbon  
78 electrode (GCE) to form a sensing platform for the detection of DA. The results  
79 demonstrated that Fe<sub>3</sub>O<sub>4</sub>@ZIF-8/RGO modified electrode had a high sensitivity,  
80 favorable performance and reproducibility, and excellent selectivity for determination  
81 of DA.

## 82 **2. Experiment**

### 83 **2.1. Materials and Reagents**

84 Ferric chloride hexahydrate (FeCl<sub>3</sub>·6H<sub>2</sub>O), sodium acetate, ethylene glycol (EG), and  
85 Zn(NO<sub>3</sub>)<sub>2</sub>·6H<sub>2</sub>O were obtained from Sinopharm Chemical Reagent, Co., Ltd  
86 (Shanghai, China). Stock solution of dopamine (0.01 mol L<sup>-1</sup>) was prepared by  
87 dissolving dopamine (0.1531 g) in 100 mL deionized water. The phosphate buffer

88 solution (PBS, 0.1 mol L<sup>-1</sup>), which was prepared by mixing Na<sub>2</sub>HPO<sub>4</sub> and NaH<sub>2</sub>PO<sub>4</sub>  
89 stock solution and adjusted to the pH value of 5.0-7.5 with 0.1 mol L<sup>-1</sup> H<sub>3</sub>PO<sub>4</sub> or  
90 NaOH solution, was used as the supporting electrolyte during all measurements.

## 91 **2.2. Apparatus**

92 The FT-IR was recorded with a Nicolet Magna-IR spectrophotometer between 4000  
93 and 450 cm<sup>-1</sup> using the KBr pellet technique. Transmission electron microscopy (TEM,  
94 FEI Tecnai G20) was obtained to elucidate the dimensions of the nanoparticle. The  
95 crystalline structures of samples were characterized by X-ray diffraction (XRD)  
96 (RigakuD/max-2400). The chemical analysis for the composites were conducted by  
97 X-ray photoelectron spectroscopy (XPS, ESCALAB210, VG, UK). Magnetization  
98 measurements were performed on a vibrating sample magnetometry (VSM,  
99 LAKESHORE-7304, USA). Amperometric measurements were performed on a CHI  
100 660E electrochemical workstation.

## 101 **2.3. Preparation of Fe<sub>3</sub>O<sub>4</sub>/RGO nanocomposites**

102 Graphite oxide (GO) was prepared according to the modified Hummers method.<sup>19</sup>  
103 Then, Fe<sub>3</sub>O<sub>4</sub>/RGO nanocomposites were synthesized via the solvothermal approach.  
104 Typically, 40 mg of GO was introduced into 30 mL of ethylene glycol (EG) and  
105 sonicated for 30 min to get brown dispersion solution. Then 0.987 g of FeCl<sub>3</sub>·6H<sub>2</sub>O  
106 and 1.946 g of sodium acetate were dissolved in the EG solution of GO by stirring for  
107 30 min. After that, the mixture was transferred to a Teflon-lined autoclave and treated  
108 at 200 °C for 8 h. The obtained Fe<sub>3</sub>O<sub>4</sub>/RGO nanocomposites were collected by  
109 magnetic decantation and washed with ethanol and distilled water thoroughly. Finally,

110 the nanocomposites were dried at 60 °C of 24 h under vacuum.<sup>20</sup>

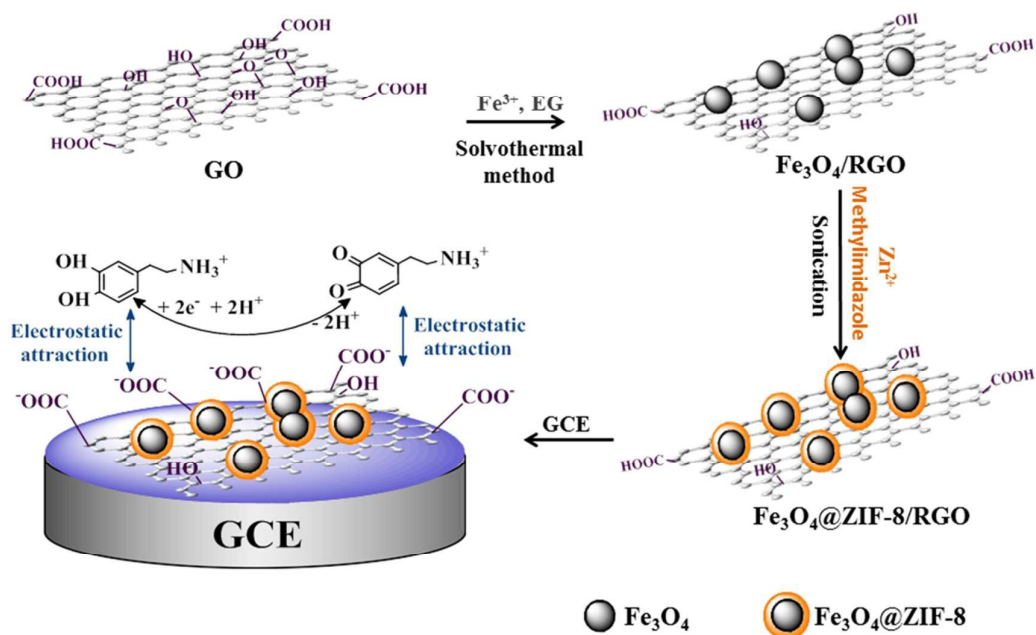
#### 111 **2.4. Preparation of Fe<sub>3</sub>O<sub>4</sub>@ZIF-8/RGO nanocomposites**

112 0.12 g of Zn(NO<sub>3</sub>)<sub>2</sub> was dissolved in 15 mL of 50% ethanol solution containing 2  
113 mmol HCl. 0.35 g of obtained Fe<sub>3</sub>O<sub>4</sub>/RGO nanocomposites was dispersed in above  
114 solution by sonication for 20 min. After that, 30 mL of 50% ethanol solution  
115 containing 0.34 g 2-methylimidazole was added to the suspension and the mixture  
116 was stirred with ultrasound at room temperature for 10 min. The product,  
117 Fe<sub>3</sub>O<sub>4</sub>@ZIF-8/RGO nanocomposites, were collected by a magnet and washed with  
118 distilled water and ethanol thoroughly, then dried at 60 °C under the vacuum for 24  
119 h.<sup>21</sup>

#### 120 **2.5. Preparation of Fe<sub>3</sub>O<sub>4</sub>@ZIF-8/RGO modified electrode**

121 1 mg of Fe<sub>3</sub>O<sub>4</sub>@ZIF-8/RGO was dispersed in 1 mL of dimethyl formamide (DMF)  
122 and the mixture was sonicated for 30 min to achieve a well-dispersed suspension.  
123 Prior to modification, the bare GCE was polished to a mirror-like surface sequentially  
124 with 1.0, 0.3 mm and 0.05 μm of α-Al<sub>2</sub>O<sub>3</sub>, and then rinsed ultrasonically with water  
125 and ethanol and de-ionized water. After the solvent was evaporated, 5 μL of  
126 Fe<sub>3</sub>O<sub>4</sub>@ZIF-8/RGO suspension was cast onto the electrode surface. Thus the  
127 Fe<sub>3</sub>O<sub>4</sub>@ZIF-8/RGO nanocomposites modified electrode (Fe<sub>3</sub>O<sub>4</sub>@ZIF-8/RGO/GCE)  
128 was obtained after it was dried in air for approximately 3 h. For comparison, the  
129 Fe<sub>3</sub>O<sub>4</sub>@ZIF-8 modified GCE (Fe<sub>3</sub>O<sub>4</sub>@ZIF-8/GCE) and GO modified GCE (GO/GCE)  
130 were prepared only by replacing the Fe<sub>3</sub>O<sub>4</sub>@ZIF-8/RGO suspension with Fe<sub>3</sub>O<sub>4</sub>@  
131 ZIF-8 or GO suspension. Fig. 1 shows the preparation of Fe<sub>3</sub>O<sub>4</sub>@ZIF-8/RGO/GCE

132 and its application for sensing analysis of DA.



133

134 Fig. 1. Scheme for the preparation of Fe<sub>3</sub>O<sub>4</sub>@ZIF-8/RGO, and its application for the

135

determination of DA.

## 136 2.6. Electrochemical measurement

137 Electrochemical characterizations of the modified electrodes were performed in

138 0.1 M phosphate buffer solution (PBS) (pH 5.0) through cyclic scan in the potential

139 range from -1.0 to 0.8 V. The electrochemical sensing test of the modified electrode

140 was carried out with a CHI 660E electrochemistry workstation by a conventional

141 three-electrode system, comprising a platinum wire as the auxiliary electrode, a

142 saturated calomel electrode as the reference electrode and the modified GCE as the

143 working electrode in the following procedure: A 15 mL solution containing an

144 appropriate amount of dopamine and 0.1 M PBS was transferred into a voltammetric

145 cell, and then cyclic voltammetry (CV) and differential-pulse voltammetry (DPV)

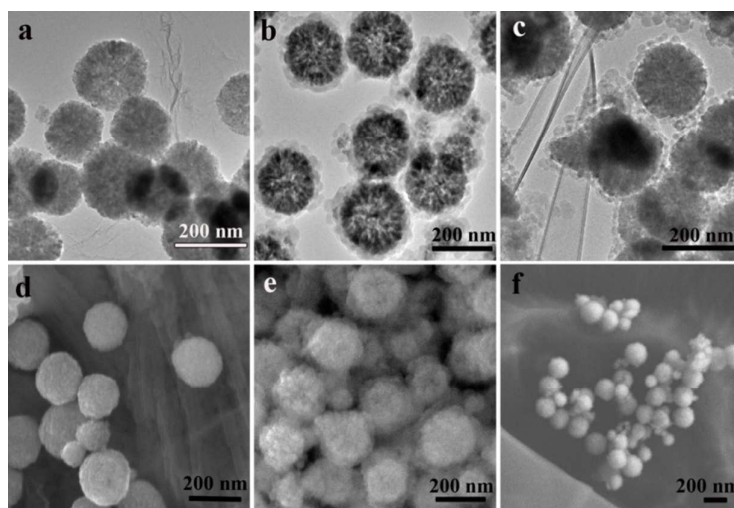
146 measurements were recorded. Real samples determination was experimented by the

147 standard addition method. The urine and serum samples were diluted with PBS (0.1  
148 M, pH 5.5) and spiked with different amounts of known concentrations of DA, and  
149 measured under the optimal conditions.

### 150 **3. Results and discussion**

#### 151 **3.1. Characterization of Fe<sub>3</sub>O<sub>4</sub>@ZIF-8/RGO nanocomposites**

152 The morphologies of the Fe<sub>3</sub>O<sub>4</sub>/RGO, Fe<sub>3</sub>O<sub>4</sub>@ZIF-8 and Fe<sub>3</sub>O<sub>4</sub>@ZIF-8/RGO are  
153 characterized by SEM and TEM, and the TEM and SEM images of each synthesized  
154 composites are shown in Fig. 2. As shown in Fig. 2a and d, Fe<sub>3</sub>O<sub>4</sub> nanoparticles have  
155 been decorated on the surface of graphene nano-sheets with a diameter of about 200  
156 nm. The monodisperse core-shell structure of Fe<sub>3</sub>O<sub>4</sub>@ZIF-8 is just like the reported.<sup>21</sup>  
157 The nearly spherical shape of Fe<sub>3</sub>O<sub>4</sub>@ZIF-8 and the formation of the ZIF-8 shell  
158 could be observed by the SEM image (Fig. 2b) and TEM image (Fig. 2e). Compared  
159 with Fe<sub>3</sub>O<sub>4</sub>/RGO and Fe<sub>3</sub>O<sub>4</sub>@ZIF-8, the Fe<sub>3</sub>O<sub>4</sub>@ZIF-8/RGO nanocomposites (Fig. 2c  
160 and f) combined two features of each composites, the folds of graphene sheets and  
161 core-shell structure of Fe<sub>3</sub>O<sub>4</sub>@ZIF-8 are exhibited obviously in the images. Therefore,  
162 demonstrated by TEM and SEM results, the novel Fe<sub>3</sub>O<sub>4</sub>@ZIF-8/RGO  
163 nanocomposites have been successfully prepared.



164

165

Fig. 2. TEM images of the  $\text{Fe}_3\text{O}_4/\text{RGO}$  (a),  $\text{Fe}_3\text{O}_4@\text{ZIF-8}$  (b) and

166

$\text{Fe}_3\text{O}_4@\text{ZIF-8}/\text{RGO}$  (c) and SEM images of the  $\text{Fe}_3\text{O}_4/\text{RGO}$  (d),  $\text{Fe}_3\text{O}_4@\text{ZIF-8}$  (e)

167

and  $\text{Fe}_3\text{O}_4@\text{ZIF-8}/\text{RGO}$  (f)

168

The chemical structures of the  $\text{Fe}_3\text{O}_4$ ,  $\text{Fe}_3\text{O}_4/\text{RGO}$ ,  $\text{Fe}_3\text{O}_4@\text{ZIF-8}$  and

169

$\text{Fe}_3\text{O}_4@\text{ZIF-8}/\text{RGO}$  are characterized by FT-IR spectra, as presented in Fig. 3. The

170

spectrum of  $\text{Fe}_3\text{O}_4$  is just same to the report, and the peak at  $580\text{ cm}^{-1}$  is related to the

171

vibration of Fe-O functional groups.<sup>22</sup> While in the FT-IR spectrum of  $\text{Fe}_3\text{O}_4/\text{RGO}$ ,

172

the bands at  $3490\text{ cm}^{-1}$  and  $1200\text{ cm}^{-1}$  appear, which correspond to the stretching

173

vibration of C-H and C-N (in the -C-NH-C- group), respectively.<sup>23, 24</sup> Compared to the

174

spectrum of  $\text{Fe}_3\text{O}_4$ , the spectrum of  $\text{Fe}_3\text{O}_4@\text{ZIF-8}$  displays different peaks contributed

175

by the ZIF-8 shell. The bands in region of  $900\text{-}1330\text{ cm}^{-1}$  and band at  $1440\text{ cm}^{-1}$  are

176

attributed to the imidazole ring, and the band at  $422\text{ cm}^{-1}$  could be assigned to the

177

Zn-N stretch mode.<sup>21, 25</sup> The spectrum of  $\text{Fe}_3\text{O}_4@\text{ZIF-8}/\text{RGO}$  nanocomposites also

178

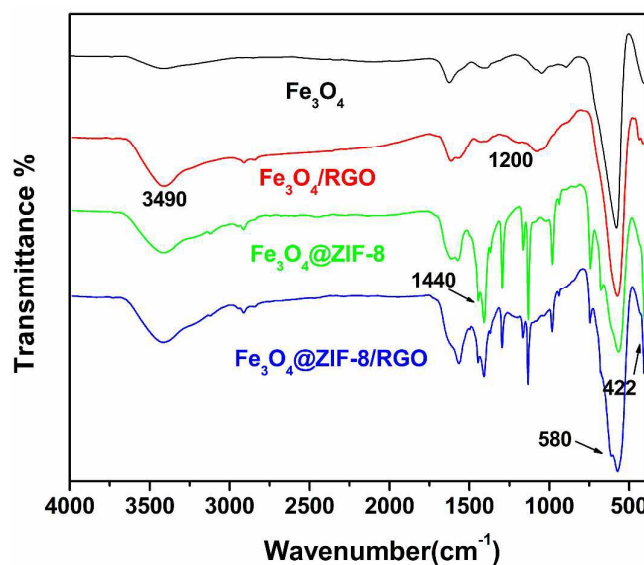
combines the features of above composites, and shows the characteristic absorption

179

bands of each constituent part. Overall, the FT-IR spectra confirmed the formation of

180

$\text{Fe}_3\text{O}_4@\text{ZIF-8}/\text{RGO}$  structure.



181

182

Fig. 3. FT-IR spectrum of Fe<sub>3</sub>O<sub>4</sub>, Fe<sub>3</sub>O<sub>4</sub>@ZIF-8, Fe<sub>3</sub>O<sub>4</sub>/RGO and

183

Fe<sub>3</sub>O<sub>4</sub>@ZIF-8/RGO nanocomposite

184

185

186

187

188

189

190

191

192

193

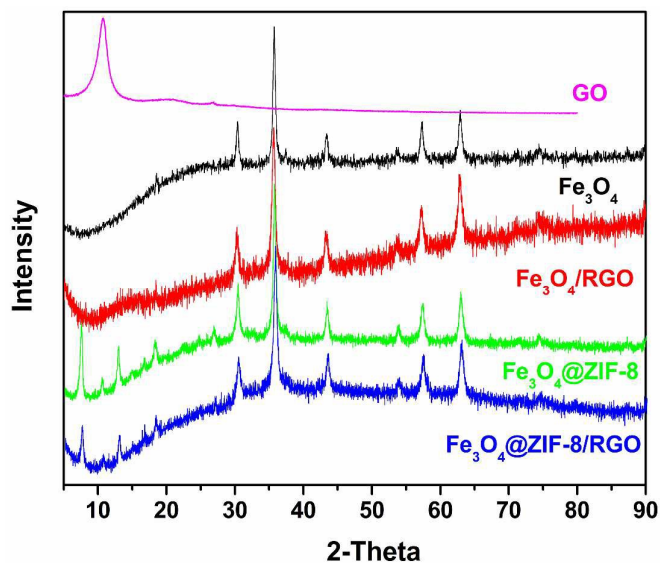
194

195

196

The crystal structure of the as prepared samples have been identified by X-ray power diffraction techniques and the XRD spectrum are show in Fig. 4. The intense and sharp peak at 10.6° in the spectrum of GO is attributed to the crystalline plane of graphite oxide, and the diffraction peaks of Fe<sub>3</sub>O<sub>4</sub> can be assigned to a superposition of standard XRD pattern of face-centered cubic Fe<sub>3</sub>O<sub>4</sub>.<sup>26</sup> However, the peak at 10.6° has entirely disappeared after the Fe<sub>3</sub>O<sub>4</sub> decorated on the graphene through hydrothermal reaction because EG could reduce GO and Fe<sup>3+</sup> to graphene and Fe<sup>2+</sup>, respectively.<sup>20, 27</sup> Simultaneously, standard Fe<sub>3</sub>O<sub>4</sub> XRD pattern in the spectrum of Fe<sub>3</sub>O<sub>4</sub>/RGO demonstrating the Fe<sub>3</sub>O<sub>4</sub> nanoparticles are successfully decorated on graphene sheets. The XRD pattern of Fe<sub>3</sub>O<sub>4</sub>@ZIF-8 is consistent with the characteristic peaks of Fe<sub>3</sub>O<sub>4</sub> and the simulated pattern of published ZIF-8 structure data.<sup>21, 28</sup> The diffraction peaks of Fe<sub>3</sub>O<sub>4</sub>@ZIF-8/RGO are very similar to Fe<sub>3</sub>O<sub>4</sub>@ZIF-8, indicating the coexistence of Fe<sub>3</sub>O<sub>4</sub>@ZIF-8 and graphene in the

197 resulted nanocomposite.



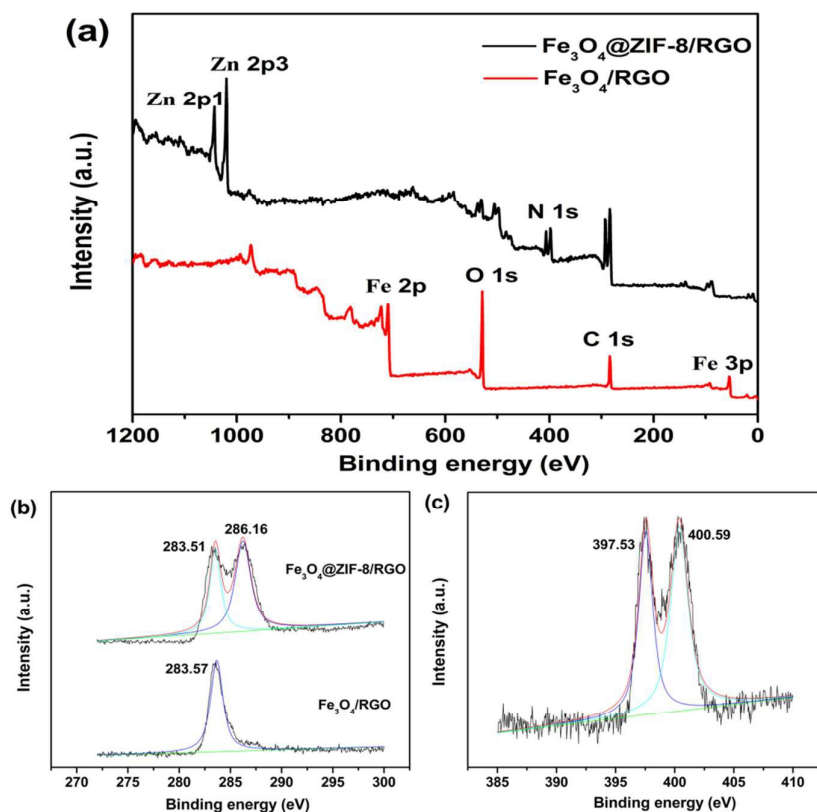
198

199 Fig. 4. XRD spectrum of Fe<sub>3</sub>O<sub>4</sub>, Fe<sub>3</sub>O<sub>4</sub>@ZIF-8, Fe<sub>3</sub>O<sub>4</sub>/RGO and

200 Fe<sub>3</sub>O<sub>4</sub>@ZIF-8/RGO nanocomposite

201 To investigate the chemical elements on the surface of the Fe<sub>3</sub>O<sub>4</sub>/RGO and  
202 Fe<sub>3</sub>O<sub>4</sub>@ZIF-8/RGO, the XPS analysis was performed. The wide-scan XPS spectra for  
203 Fe<sub>3</sub>O<sub>4</sub>/RGO and Fe<sub>3</sub>O<sub>4</sub>@ZIF-8/RGO are shown in Fig. 5(a). The characteristic peaks  
204 of Fe 2p, Fe 3p, O 1s and C 1s appeared in the spectrum of Fe<sub>3</sub>O<sub>4</sub>/RGO. Compared  
205 with the Fe<sub>3</sub>O<sub>4</sub>/RGO, new peaks assigned to Zn 2p<sub>1</sub>, Zn 2p<sub>3</sub> and N 1s are clearly  
206 observed in the spectrum of Fe<sub>3</sub>O<sub>4</sub>@ZIF-8/RGO, demonstrated the MOFs (ZIF-8)  
207 have been successfully reacted on the surface of Fe<sub>3</sub>O<sub>4</sub>. Moreover, as the ZIF-8 was  
208 covered on the Fe<sub>3</sub>O<sub>4</sub>, the peaks of Fe 2p and Fe 3p are disappeared and the peak of O  
209 1s decreased sharply. Fig. 5(b) shows the C 1s spectrums of Fe<sub>3</sub>O<sub>4</sub>/RGO and  
210 Fe<sub>3</sub>O<sub>4</sub>@ZIF-8/RGO, the only peak at 527.95 eV could be assigned to the C-C in the  
211 spectrum of Fe<sub>3</sub>O<sub>4</sub>/RGO, and two peaks in Fe<sub>3</sub>O<sub>4</sub>@ZIF-8/RGO corresponding to C-C  
212 (183.51 eV) and C=C (186.16 eV) demonstrated the 2-methylimidazole has covered

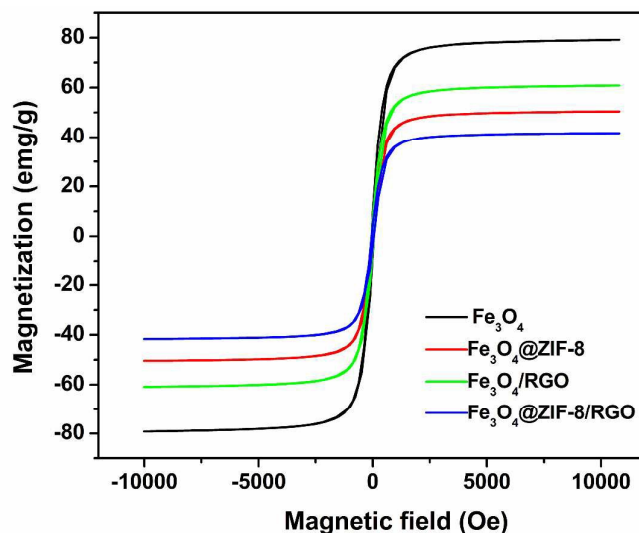
213 on the  $\text{Fe}_3\text{O}_4$ . The N 1s spectrum of  $\text{Fe}_3\text{O}_4@\text{ZIF-8}/\text{RGO}$  (Fig. 6(c)) shows two species  
 214 of N 1s peak corresponding to  $-\text{NH}-$  (397.53 eV) and  $-\text{N}=$  (400.59 eV) which also  
 215 characterized the 2-methylimidazole on the nanocomposite.<sup>20, 29</sup>



216  
 217 Fig. 5. XPS spectra of (a) wide scan of  $\text{Fe}_3\text{O}_4/\text{RGO}$  and  $\text{Fe}_3\text{O}_4@\text{ZIF-8}/\text{RGO}$ ; (b) N  
 218 1s of  $\text{Fe}_3\text{O}_4@\text{ZIF-8}/\text{RGO}$ ; (c) C1s of  $\text{Fe}_3\text{O}_4/\text{RGO}$  and  $\text{Fe}_3\text{O}_4@\text{ZIF-8}/\text{RGO}$

219 The magnetic property of  $\text{Fe}_3\text{O}_4@\text{ZIF-8}/\text{RGO}$  was studied using a superconducting  
 220 quantum interference device (SQUID) magnetometer at room temperature, as shown  
 221 in Fig. 6. The hysteresis loops of the  $\text{Fe}_3\text{O}_4$  nanoparticle,  $\text{Fe}_3\text{O}_4/\text{RGO}$ ,  $\text{Fe}_3\text{O}_4@\text{ZIF-8}$   
 222 and  $\text{Fe}_3\text{O}_4@\text{ZIF-8}/\text{RGO}$  nanocomposite are characterized the magnetic measurements  
 223 of each product. The saturation magnetization of  $\text{Fe}_3\text{O}_4$ ,  $\text{Fe}_3\text{O}_4/\text{RGO}$ ,  $\text{Fe}_3\text{O}_4@\text{ZIF-8}$   
 224 and  $\text{Fe}_3\text{O}_4@\text{ZIF-8}/\text{RGO}$  is 79.08, 60.87, 50.41 and 41.65  $\text{emu g}^{-1}$ , respectively.  
 225 Although the magnetic intensity of  $\text{Fe}_3\text{O}_4@\text{ZIF-8}/\text{RGO}$  decreases obviously after the

226 ZIF-8 was reacted on the  $\text{Fe}_3\text{O}_4$ , the  $\text{Fe}_3\text{O}_4@\text{ZIF-8}/\text{RGO}$  nanocomposite can be easily  
227 separated conveniently by using magnetic field, and facilitated collection and  
228 operation.<sup>30</sup>



229

230 Fig. 6. VSM curves (B) of  $\text{Fe}_3\text{O}_4$ ,  $\text{Fe}_3\text{O}_4@\text{ZIF}$ ,  $\text{Fe}_3\text{O}_4/\text{RGO}$  and

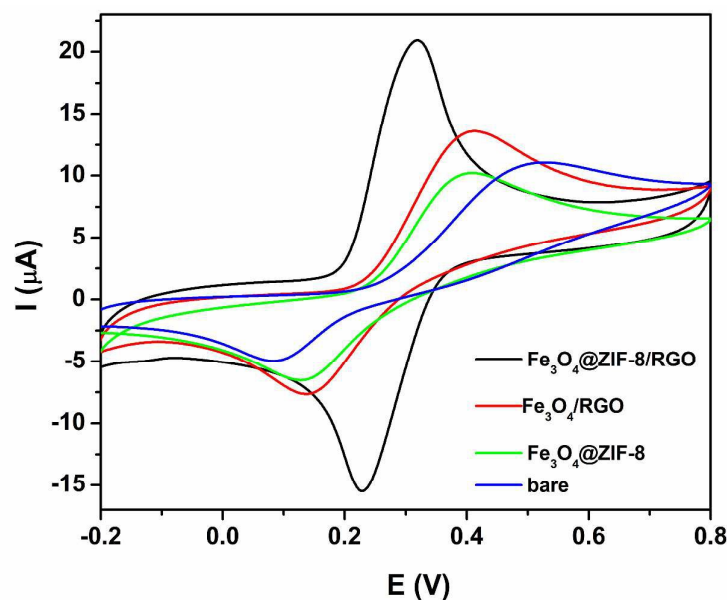
231

$\text{Fe}_3\text{O}_4@\text{ZIF-8}/\text{RGO}$  nanocomposite

### 232 3.2. Voltammetric behavior of DA at $\text{Fe}_3\text{O}_4@\text{ZIF-8}/\text{RGO}/\text{GCE}$

233 To exploit the potential application of the  $\text{Fe}_3\text{O}_4@\text{ZIF-8}/\text{RGO}$  nanocomposite,  
234 the electrochemical behaviors of DA were investigated on the  $\text{Fe}_3\text{O}_4@\text{ZIF-8}/\text{RGO}$   
235 /GCE. Fig. 7 shows typical CVs of 1 mM DA on the bare GCE, the  $\text{Fe}_3\text{O}_4@\text{ZIF-8}$   
236 /GCE, the  $\text{Fe}_3\text{O}_4/\text{RGO}/\text{GCE}$  and the  $\text{Fe}_3\text{O}_4@\text{ZIF-8}/\text{RGO}/\text{GCE}$ . On the bare GCE, DA  
237 exhibits a reversible electrochemical behavior and the small current indicates it is  
238 inefficient to detect of DA on the bare GCE. At the  $\text{Fe}_3\text{O}_4@\text{ZIF-8}$ , a couple of small  
239 redox peaks appeared and the oxidation peak current of DA enhanced notable, it is  
240 because that the relative large surface area of electrode increased significantly after  
241 immobilization of  $\text{Fe}_3\text{O}_4@\text{ZIF-8}$ . Due to the excellent electric conductivity of reduced

242 graphite oxide, the anodic peak current at the  $\text{Fe}_3\text{O}_4/\text{RGO}/\text{GCE}$  is increased strikingly.  
243 However, when the  $\text{Fe}_3\text{O}_4@\text{ZIF-8}/\text{RGO}/\text{GCE}$  was applied for determination, the  
244 redox peaks of DA increased dramatically with a well-defined peak shape, and the  
245 redox process became more reversible as judged from the more symmetric peak  
246 profiles. Therefore, the component of MOFs (ZIF-8) material in the graphene  
247 nano-sheets have positive effect on improving the electrochemical response, which is  
248 likely caused by the outstanding porous structure and favorable electron transfer  
249 mediating function of the electroactive MOFs.<sup>7,31</sup>



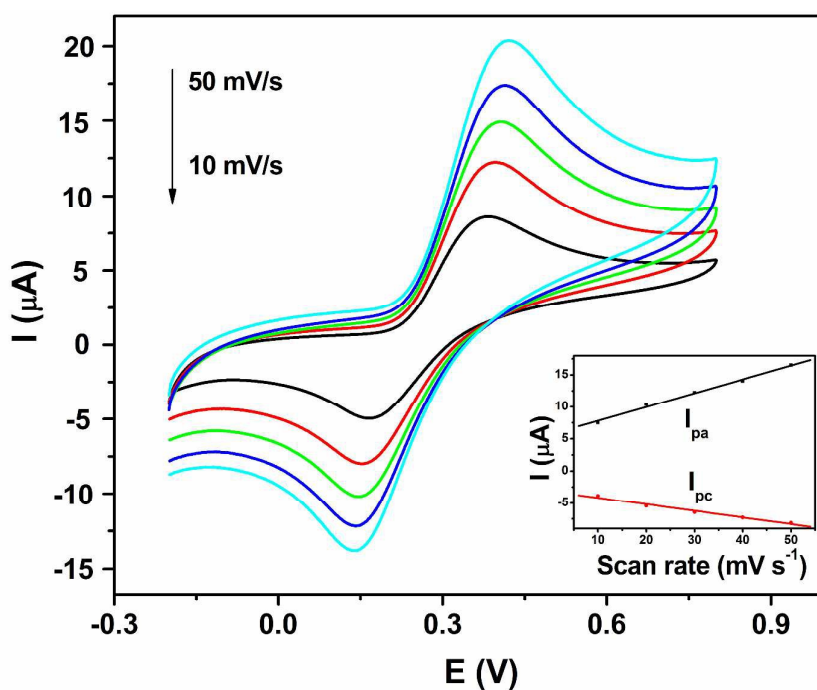
250

251 Fig. 7. Cyclic voltammograms at the are GCE, the  $\text{Fe}_3\text{O}_4@\text{ZIF-8}/\text{GCE}$ , the  
252  $\text{Fe}_3\text{O}_4/\text{RGO}/\text{GCE}$  and the  $\text{Fe}_3\text{O}_4@\text{ZIF-8}/\text{RGO}/\text{GCE}$  in the presence of DA in PBS  
253 (0.1M, pH 5.5). DA concentration: 1 mM, and scan rate:  $20 \text{ mV s}^{-1}$

### 254 3.3. Electrochemical parameters of DA at $\text{Fe}_3\text{O}_4@\text{ZIF-8}/\text{RGO}/\text{GCE}$

255 The influence of the scan rate ( $v$ ) on the oxidation current of 0.1 mM DA was  
256 examined using  $\text{Fe}_3\text{O}_4@\text{ZIF-8}/\text{RGO}/\text{GCE}$  in 0.1 M pH 5.0 PBS by varying the scan

257 rates from 10 to 50  $\text{mV s}^{-1}$ . As shown in Fig. 8, the anodic and cathodic peak currents  
258 are both increased gradually when increasing the scan rate. Farther more, with the  
259 increase of scan rate, the anodic peak potential and cathodic peak potential slightly  
260 shifted to more positive and negative potentials, respectively, indicating that the  
261 electrontransfer rate decreased and the electrochemical reaction of DA tended to be  
262 less reversible. A good linear relationship among the scan rate, the values of the  
263 anodic peak current ( $I_{\text{pa}}$ ) and the cathodic peak current ( $I_{\text{pc}}$ ) is also obtained. The  
264 linear regression equation for the anodic peak current and cathodic current is  $I_{\text{pa}} (\mu\text{A})$   
265  $= 5.6328 + 0.21468v (\text{mV s}^{-1})$ , and  $I_{\text{pc}} (\mu\text{A}) = -3.1756 - 0.1023v (\text{mV s}^{-1})$ , respectively,  
266 and the correlation coefficient is  $R_{\text{pa}} = 0.9965$ ,  $R_{\text{pc}} = 0.9903$ , respectively. This result  
267 suggests that the electrochemical oxidation is an absorption-controlled process for DA  
268 at the  $\text{Fe}_3\text{O}_4@\text{ZIF-8}/\text{RGO}/\text{GCE}$  surface.<sup>32</sup>



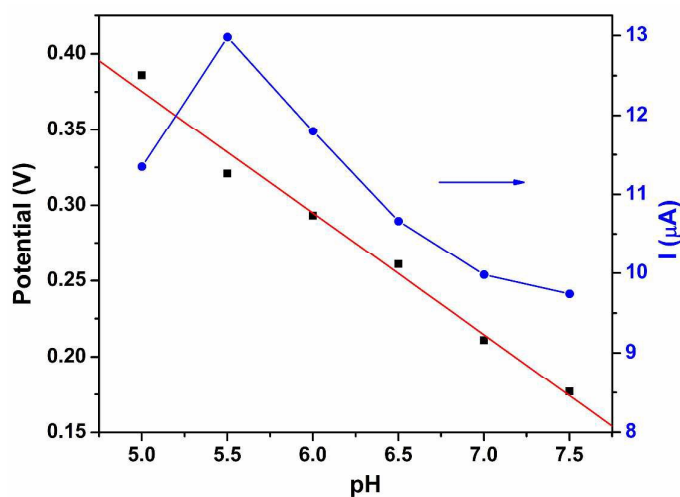
269

270

Fig. 8. Cyclic voltammograms of 0.1 mM DA in 0.1 mM PBA at the

271  $\text{Fe}_3\text{O}_4@\text{ZIF-8}/\text{RGO}/\text{GCE}$  at scan rate of  $10\text{-}50\text{ mV s}^{-1}$ . The inset shows the plots of  
272 anodic and cathodic peak currents *vs.* scan rates.

273 Since the redox system was affected by the change of pH due to the involvement of  
274 protons in the electrode reaction and the electro-catalytic reaction at the  
275  $\text{Fe}_3\text{O}_4@\text{ZIF-8}/\text{RGO}/\text{GCE}$  is a two electron, two proton process, the influence of pH  
276 on the biosensor performance was investigated by measuring the electrode response in  
277  $0.1\text{ mM}$  DA with pH values ranging from 5.0 to 7.5.<sup>33</sup> As shown in Fig. 9, the  
278 oxidation peak potential ( $E_{\text{pa}}$ ) of DA shifted negatively with the increased of pH. A  
279 good linear relationship between  $E_{\text{pa}}$  and pH was constructed and described with a  
280 linear equation:  $E(\text{V}) = -0.0704\text{ pH} + 0.7773$  ( $R=0.9935$ ). Farther more, the oxidation  
281 peak current ( $I_{\text{pa}}$ ) also changed with the pH of DA solution ranged from 5.0 to 7.5,  
282 and the maximum response current was obtained at pH of 5.5. Thus, a phosphate  
283 buffer solution of pH 5.5 was chosen as the optimum pH and used in all experiments  
284 below.



285

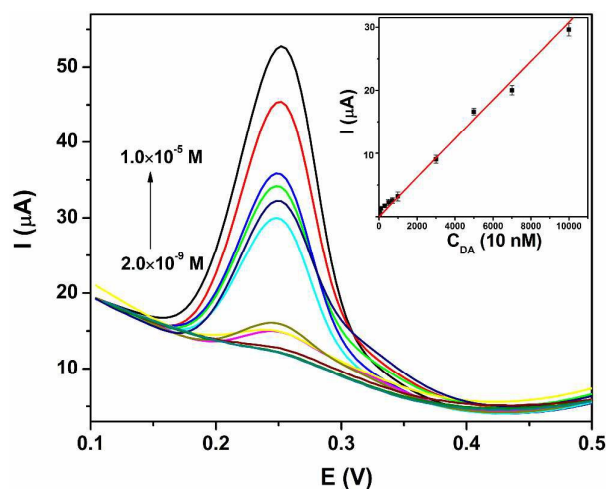
286 Fig. 9. Effects of pH on  $E_{\text{pa}}$  and  $I_{\text{pa}}$  of  $0.1\text{ mM}$  in  $0.1\text{ M}$  PBS on the

287

$\text{Fe}_3\text{O}_4@\text{ZIF-8}/\text{RGO}/\text{GCE}$

### 3.4. Analytical performance and applications

Voltammetric current responses of successive additions of DA were recorded by differential pulse voltammetry (DPV) to check the sensitivity of the sensor under the optimal experimental conditions. As shown in Fig. 10, with the increasing concentration of DA, the oxidation peak current ( $I_{pa}$ ) increased relatively. Linearly proportional of peak current and DA concentration is observed in the range from  $2.0 \times 10^{-9}$  to  $1.0 \times 10^{-5}$  M (inset of Fig. 10). The linear regression equations for DA is  $I_{pa}$  ( $\mu\text{A}$ ) =  $1.144 + 0.0056C$  ( $10^{-9}$  M) and the correlation coefficient is 0.9966. According to signal to noise (S/N) = 3, the detection limits of DA was estimated to be  $6.67 \times 10^{-10}$  M. Table 1 summarized the comparison of analytical results of the analytical performance  $\text{Fe}_3\text{O}_4@\text{ZIF-8}/\text{RGO}/\text{GCE}$  with other dopamine sensor reported recently. Through the comparison, the obtained biosensor in this work has comparable and even better performance than the others, demonstrating that  $\text{Fe}_3\text{O}_4@\text{ZIF-8}/\text{RGO}/\text{GCE}$  has extraordinary application potential in determination of DA.



302

303 Fig. 10. DPV for different concentration of DA at the  $\text{Fe}_3\text{O}_4@\text{ZIF-8}/\text{RGO}/\text{GCE}$ .

304 The inset shows the relationship between the peak current and DA concentration

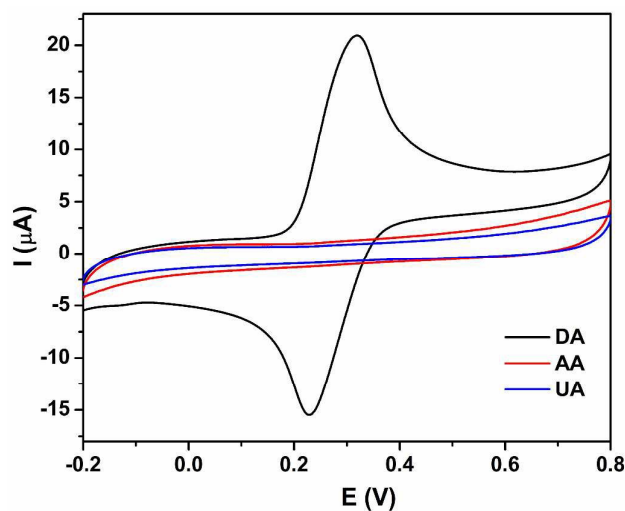
305

306 **Table 1** Comparison of analytical performance of DA at different modified electrodes

Modified materials	Methods	Linear ranges (M)	Detection limits (M)	reference
GO	DPV	$1 \times 10^{-6}$ - $1.5 \times 10^{-7}$	$0.27 \times 10^{-6}$	35
Fe <sub>3</sub> O <sub>4</sub> /r-GO	DPV	$4 \times 10^{-7}$ - $1.6 \times 10^{-4}$	$8 \times 10^{-8}$	36
Pd/graphene/chitosan	DPV	$5 \times 10^{-7}$ - $2 \times 10^{-4}$	$1 \times 10^{-7}$	37
Polypyrrole@r-GO	DPV	$6 \times 10^{-8}$ - $8 \times 10^{-6}$	$6 \times 10^{-9}$	38
Cu(tpa)-EGR	DPV	$1 \times 10^{-6}$ - $5 \times 10^{-5}$	$2.1 \times 10^{-7}$	7
Nafion/C/Al-MIL-53-(OH) <sub>2</sub>	DPV	$3 \times 10^{-8}$ - $1 \times 10^{-5}$	$8 \times 10^{-9}$	8
Porphyrin-RGO	DPV	$1 \times 10^{-6}$ - $7 \times 10^{-5}$	$9.5 \times 10^{-9}$	39
RGO-MWNTs-PTA	DPV	$5 \times 10^{-7}$ - $2 \times 10^{-5}$	$1.14 \times 10^{-6}$	40
Fe <sub>3</sub> O <sub>4</sub> @ZIF-8/RGO	DPV	$2 \times 10^{-9}$ - $1 \times 10^{-5}$	$6.67 \times 10^{-10}$	This work

307 As an important parameter for a biosensor, discriminating the target between the  
308 interfering species in similar physiological environments is necessary to be  
309 investigated. For the determination of DA, the electrochemical behaviors of ascorbic  
310 acid (AA), and uric acid (UA) (usually coexist with DA) on Fe<sub>3</sub>O<sub>4</sub>@ZIF-8/RGO/GCE  
311 has been studied. As shown in Fig. 11, a couple of shape redox peaks is exhibited in the  
312 CV of 1 mM of DA, on the contrary, no obvious peak appeared in the CV of  $1 \times 10^{-3}$  M  
313 of AA and UA, which suggested that DA can be detected in the presence of AA and  
314 UA.<sup>34</sup> To demonstrate the selectivity of Fe<sub>3</sub>O<sub>4</sub>@ZIF-8/RGO/GCE for DA more  
315 comprehensively, various potential organic compounds and inorganic ions such as  
316 NaCl, K<sub>2</sub>SO<sub>4</sub>, CaCl<sub>2</sub> solutions, lysine, cysteine and glucose solutions were added to  
317 the 1 mM of DA solution. The peak currents of DA showed almost no interference in  
318 the presence of these influences since their peak current changes were below 5%. A  
319 possible reaction mechanism was discussed here, the negatively charged  
320 Fe<sub>3</sub>O<sub>4</sub>@ZIF-8/RGO acted as electro-catalysts and selective reagents simultaneously,

321 thus, the positively charged DA was attracted and electro-catalyzed on the sensor,  
322 otherwise, the negatively charged analytes such as AA and UA were repelled.  
323 Therefore, with a wide linear range, low detection potential, and high sensitivity, the  
324  $\text{Fe}_3\text{O}_4@\text{ZIF-8}/\text{RGO}$  could be used as promising candidates to prepare the dopamine  
325 biosensors.



326  
327 Fig. 11. Cyclic voltammograms of the  $\text{Fe}_3\text{O}_4@\text{ZIF-8}/\text{RGO}/\text{GCE}$  in 0.1 PBS with 1  
328 mM DA, AA and UA, respectively.

### 329 3.5. Reproducibility of biosensor and real sample determination.

330 The reproducibility and stability of the  $\text{Fe}_3\text{O}_4@\text{ZIF-8}/\text{RGO}/\text{GCE}$  were further  
331 examined. When the electrode was successively scanned in 1 mM DA in 0.1 M pH  
332 5.0 PBS for 50 cycles, there were no obvious changes in the peak current in the CV  
333 curves. Repeated DPV experiment was also conducted in the same condition, and the  
334 relative standard deviation (RSD) was 2.13% after 15 successive measurements. The  
335 long-term stability of the electrode was investigated by measuring its CV response  
336 over a 10 day period. The fabricated electrodes were stored under normal conditions  
337 at room temperature, and no obvious changes were found when measured it

338 periodically. Therefore, the results indicated the excellent reproducibility and stability  
 339 of the prepared Fe<sub>3</sub>O<sub>4</sub>@ZIF-8/RGO/GCE biosensor. Real samples were analyzed by  
 340 the standard addition method to evaluate the potential application of  
 341 Fe<sub>3</sub>O<sub>4</sub>@ZIF-8/RGO/GCE biosensor. Urine and serum samples were diluted with PBS  
 342 (0.1 M, pH 5.5) in order to avoid the interferences of the complicated matrix in the  
 343 real samples and fit into the linear ranges of DA. Then the diluted samples were  
 344 spiked with different amounts of known concentrations of DA, and measured under  
 345 the optimal conditions. The analytical results are shown in Table 2. As can be  
 346 observed, the recovery of the spiked samples was in the range of 98.20-102.73% (n =  
 347 5) with the relative standard derivation (RSD) values were calculated to be less than  
 348 2.69%, indicated that the method is reliable and sensitive for determination of DA in  
 349 real samples.

350 **Table 2** Determination of DA in real samples using Fe<sub>3</sub>O<sub>4</sub>@ZIF-8/RGO/GCE

Samples	Added ( $\mu$ M)	Found ( $\mu$ M)	RSD (%)	Recovery (%)
Serum 1	—	0.093	1.91	—
	0.200	0.301	2.23	102.73
	0.500	0.597	2.54	100.81
Serum 2	—	0.223	2.36	—
	0.200	0.429	1.87	101.42
	0.500	0.719	1.61	99.44
Urine 1	—	0.134	2.62	—
	0.200	0.328	2.69	98.20
	0.500	0.639	2.28	100.88
Urine 2	—	1.102	1.77	—
	0.200	1.309	1.89	100.73
	0.500	1.597	2.01	99.61

#### 351 4. Conclusions

352 In this paper, a novel hybrid nanocomposite of magnetic Fe<sub>3</sub>O<sub>4</sub>@ZIF-8 decorated

353 graphene was prepared by a simple method for the first time. After the Fe<sub>3</sub>O<sub>4</sub>/RGO  
354 was formed by solvothermal approach, the MOFs (ZIF-8) was fabricated on the  
355 surface of Fe<sub>3</sub>O<sub>4</sub> to get the Fe<sub>3</sub>O<sub>4</sub>@ZIF-8/RGO nanocomposite. By combing the  
356 unique properties of large specific surface area and high conductivity derived from  
357 both of MOFs and graphene, the Fe<sub>3</sub>O<sub>4</sub>@ZIF-8/RGO nanocomposites modified glassy  
358 carbon electrode was successfully constructed and used for electrochemical detection  
359 of DA. The fabricated biosensor showed great potential applications in the detection  
360 of DA with extraordinary advantages such as wide linear range ( $2.0 \times 10^{-9}$ – $1.0 \times 10^{-5}$  M),  
361 low detection limit ( $6.67 \times 10^{-10}$ ) and good selectivity for DA detection in the presence  
362 of ascorbic acid and uric acid. Moreover, the prepared sensor also showed satisfactory  
363 result in real samples detection. Our present study demonstrated the combination of  
364 MOFs and graphene composites could fabricate a new kind of high sensitive  
365 biosensor for electrochemical detection.

#### 366 **Acknowledgments**

367 The authors gratefully acknowledge financial supports from the National Natural  
368 Science Foundation of China (No. 21304040), Natural Science Foundation of Gansu  
369 Province (1308RJYA027) and Chinese Postdoctoral Funds (2013M532090). This  
370 paper is dedicated to memory of pro. Yanfeng Li, who passed away recently.

371

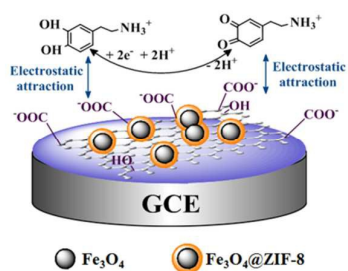
## Reference

- 1 J. R. Li, J. Sculley and H. C. Zhou, *Chem. Rev.*, 2011, **112**, 869.
- 2 M. Yaghi, M. O’Keeffe, N. W. Ockwig, H. K. Chae, M. Eddaoudi and J. Kim, *Nature*, 2003, **423**, 705.
- 3 P. Chowdhury, C. Bikkina, D. Meister, F. Dreisbach and S. Gumma, *Microporous Mesoporous Mater.*, 2009, **117**, 406.
- 4 M. Zhao, S. Ou and C. D. Wu, *Acc. Chem. Res.*, 2014, **47**, 1199.
- 5 Y. Li, C. Huangfu, H. Du, W. Liu, Y. Li and J. Ye, *J. Electroanal. Chem.*, 2013, **709**, 65.
- 6 Y. Zhang, X. Bo, C. Luhana, H. Wang, M. Li and L. Guo, *Chem. Commun.*, 2013, **49**, 6885.
- 7 X. Wang, Q. X. Wang, Q. H. Wang, F. Gao, F. Gao, Y. Z. Yang and H. X. Guo, *ACS Appl. Mat. Interfaces*, 2014, **6**, 11573.
- 8 Y. Wang, H. L. Ge, G. Q. Ye, H. H. Chen and X. Y. Hu, *J. Mater. Chem. B*, 2015, **3**, 3747.
- 9 X. Li, S. Zhu, B. Xu, K. Ma, J. Zhang, B. Yang and W. Tian, *Nanoscale*, 2013, **5**, 7776.
- 10 L. Li, A. R. O. Raji and J. M. Tour, *Adv. Mater.*, 2013, **25**, 6298.
- 11 B. Zhan, C. Liu, H. Chen, H. Shi, L. Wang, P. Chen, W. Huang and X. Dong, *Nanoscale*, 2014, **6**, 7424.
- 12 C. Z. Liao, M. Zhang, L. Y. Niu, Z. j. Zheng and F. Yan, *J. Mater. Chem. B*, 2014, **2**, 191-200.
- 13 X. M. Feng, Y. Zhang, J. h. Zhou, Y. Li, S. F. Chen, L. Zhang, Y. W. Ma, L. H. Wang and X. H. Yan, *Nanoscale*, 2015, **7**, 2427.
- 14 A. M. J. Haque, H. Park, D. Sung, S. Jon, S. Y. Choi and K. Kim, *Anal. Chem.*, 2012, **84**, 1871.
- 15 X. H. Li, H. Zhu, J. Feng, J. Zhang, X. Deng, B. Zhou, H. Zhang, D. Xue, F. Li, N. Mellors, Y. F. Li and Y. Peng, *carbon*, 2013, **60**, 488.

- 16 S. Ikemoto, *Brain Res. Rev.*, 2007, **56**, 27.
- 17 W. X. Zhang, J. Z. Zheng, C. H. Tan, X. Lin, Sh. R. Hu, J. H. Chen, X. L. You and S. X. Li, *J. Mater. Chem. B*, 2015, **3**, 217-224.
- 18 Y. C. Pan, Y. Y. Liu, G. F. Zeng, L. Zhao and Z. P. Lai, *Chem. Commun.*, 2011, **47**, 2071.
- 19 H. Zhou, W. Yao, G. Li, J. Wang and Y. Lu, *Carbon*, 2013, **59**, 495.
- 20 W. Yao, T. Ni, S. Chen, H. Li and Y. Lu, *Compos. Sci. Technol.*, 2014, **99**, 15.
- 21 J. N. Zheng, Z. Lin, G. Lin, H. H. Yang and L. Zhang, *J. Mater. Chem. B*, 2015, **3**, 2185.
- 22 Y. Wang, Y. Zhang, C. Hou, Z. Qi, X. He, *Chemosphere*, 2015, **141**, 26.
- 23 Y. Q. Wang, B. F. Zou, T. Gao, X. P. Wu, S. Y. Lou, S. M. J. Zhou, *Mater. Chem.*, 2012, **22**, 9034.
- 24 H. L. Ma, Y. W. Zhang, Q. H. Hu, D. Yan, Z. Z. Yu, Zhai M. L. Zhai, *J. Mater. Chem.*, 2012, **22**, 5914.
- 25 Y. Hu, H. Kazemian, S. Rohani, Y. N. Huang and Y. Song, *Chem. Commun.*, 2011, **47**, 12694.
- 26 W. Fan, W. Gao, C. Zhang, W. W. Tjiu, J. S. Pan, T. X. Liu, *J. Mater. Chem.*, 2012, **22**, 25108.
- 27 K. F. Zhou, Y. H. Zhu, X. L. Yang, C. Z. Li, *New J. Chem.*, 2010, **34**, 2950.
- 28 K. S. Park, Z. Ni, A. P. Côté, J. Y. Choi, R. Huang, F. J. Uribe-Romo, H. K. Chae, M. O'Keeffe and O. M. Yaghi, *Proc. Natl. Acad. Sci. U. S. A.*, 2006, **103**, 10186.
- 29 L. Sun, L. Wang, C. G. Tian, T. X. Tan, Y. Xie and K. Y. Shi, *RSC Adv.*, 2012, **2**, 4498.
- 30 Y. Wang, Y. Zhang, C. Hou, X. He, M. Liu, *J. Taiwan Inst. Chem. E.*, 2015, doi:10.1016/j.jtice.2015.05.044.
- 31 C. L. Sun, H. H. Lee, J. M. Yang and C. C. Wu, *Biosens. Bioelectron.*, 2011, **26**, 3450.
- 32 M. Zheng, F. Gao, Q. Wang, X. Cai, S. Jiang, L. Huang and F. Gao, *Mater. Sci. Eng. C*, 2013,

- 33, 1514.
- 33 J. Yang, J. R. Strickler and S. Gunasekaran, *Nanoscale*, 2012, **4**, 4594.
- 34 X. Dong, X. Wang, L. Wang, H. Song, H. Zhang, W. Huang and P. Chen, *ACS Appl. Mat. Interfaces*, 2012, **4**, 3129.
- 35 F. Gao, X. Cai, X. Wang, C. Gao, S. Liu, F. Gao and Q. Wang, *Sens. Actuators, B*, 2013, **186**, 380.
- 36 H. Teymourian, A. Salimi and S. Khezrian, *Biosens. Bioelectron.*, 2013, **49**, 1.
- 37 X. Wang, M. Wu, W. Tang, Y. Zhu, L. W. Wang, Q. J. Wang, P. J. He and Y. Z. Fang, *J. Electroanal. Chem.*, 2013, **695**, 10.
- 38 T. Qian, S. S. Wu and J. Shen, *Chem. Commun.*, 2013, **49**, 4610.
- 39 S. F. Hou, M. L. Kasner, S. J. Su, K. Patel and R. Cuellari, *J. Phys. Chem.*, 2010, **114**, 14915.
- 40 Y. Y. Ling, Q. A. Huang, M. S. Zhu, D. X. Feng, X. Z. Li and Y. J. Wei, *Electroanal. Chem.*, 2013, **693**, 9.

Graphical abstract:



A novel hybrid nanocomposite of magnetic  $\text{Fe}_3\text{O}_4@ZIF-8$  decorated reduced graphite was prepared and used to determination of dopamine.